Biochemical and photosystem characteristics of wild-type and Chl *b*-deficient mutant in tree peony (*Paeonia suffruticosa*)

L.X. ZHANG[*,†], Q.S. CHANG[**,†,+], X.G. HOU[*,+], S.D. CHEN[**], Q.M. ZHANG[**], J.Z. WANG[***], S.D. LIU[#], and S. LI[*]

College of Agriculture, Henan University of Science and Technology, 471000 Luoyang, China[*]
College of Horticulture and Plant Protection, Henan University of Science and Technology, 471000 Luoyang, China[**]
Luoyang Greening Management Center, 471000 Luoyang, China[***]
Luoyang International Peony Garden, 471000 Luoyang, China[#]

Abstract

In order to explore the adaptive strategies of tree peony *yl1* mutant in response to photooxidative stress, the changes of biochemical parameters, chlorophyll fluorescence, and the modulated 820-nm reflection of *yl1* mutant and wild-type plants were compared. We found the activities of superoxide dismutase and catalase, the contents of soluble protein, proline, superoxide radicals, hydrogen peroxide, malondialdehyde, and relative electrical conductivity were significantly higher than those of the wild type. The photochemical efficiency of PSII significantly decreased, while the proportion of heat dissipation of *yl1* mutant increased greatly. The donor and acceptor side and electron transfer of PSII were greatly inhibited. Meanwhile, the performance of PSI and coordination of two photosystems decreased markedly in *yl1* mutant. The *yl1* mutant could reduce the damage caused by photooxidative stress by increasing the activity of antioxidant enzymes, the content of some osmoregulatory substances, and the proportion of heat dissipation.

Introduction

Leaves are the main organs of photosynthesis in higher plants, and chlorophyll (Chl) in leaves plays an important role in absorbing and converting light energy, so the biosynthesis and degradation of Chl are very important for photosynthesis of plants (Wang *et al.* 2018). The decrease of Chl content often leads to the decrease of photosynthetic capacity, poor growth, and development, and even the decrease of biomass (Liu *et al.* 2016a, Lai *et al.* 2018). Therefore, Chl-deficient mutants are ideal materials for studying the mechanism of photosynthesis, the structure and function of the photosystems, and Chl biosynthesis, and are valuable for cultivating excellent varieties and molecular marker-assisted breeding (Zhang *et al.* 2020). Leaf-color mutants with yellow leaves, variegated leaves, stripes, and other characteristics have a high ornamental value in landscaping. Among them, a yellow-leaf mutant is a common mutation type. The paulownia (*Paulownia fortnnei*) mutant with white flowers presented light green leaves at the seedling stage, they turned yellow at the mature stage, and had a certain ornamental value (Ru *et al.*

Highlights

- Higher photooxidative damage was reported in tree peony *yl1* mutant compared to the wild type.
- The function and coordination of two photosystems in *yl1* mutant decreased significantly.
- The *yl1* mutant increased the contents of antioxidants and osmoregulants and heat dissipation capacity in response to photooxidative stress.

2017). The young leaves of yellow-leaf mutant 'Golden Qilu' changed from orange yellow to golden yellow in spring, and then gradually turned green, which greatly improved the ornamental value of *Acer truncatum* (Chu 2020).

Carotenoids (Car) play an important role in protecting photosynthetic apparatus from photooxidative damage by reactive oxygen species (ROS), and some leaf-color mutants are vulnerable to oxidative stress due to concomitant lack of Car (Chai *et al.* 2011, Kalaji *et al.* 2017). The contents of malondialdehyde (MDA), hydrogen peroxide, and superoxide radical ($O_2^{\cdot-}$) in the leaves usually increase, resulting in damage to leaves (Guo 2020). Many leaf-color mutants can reduce the damage caused by ROS, prevent the aggravation of membrane lipid peroxidation, and improve resistance by increasing the contents of osmotic substances and the activities of antioxidant enzymes (Lv 2010, Li 2016). Although the content of MDA increased in the paulownia (*P. fortunei*) yellowing mutant (Ru *et al.* 2017) and the thin-skinned melon (*Cucumis melo*) natural yellowing to green mutant (Lai *et al.* 2018), the activities of superoxide dismutase (SOD), peroxidase (POD), and catalase (CAT) were markedly enhanced to reduce the damage caused by membrane lipid peroxidation.

Photosynthesis involves the absorption, transfer, and transformation of light energy, which depends on the coordination of PSII and PSI; the capture and distribution of light energy are the core of photosynthesis (Du *et al.* 2019). As a noninvasive and highly sensitive method, Chl fluorescence technique can accurately evaluate the function and structure of photosynthetic apparatus, and its measurement parameters are closely related to the function of PSII (Dąbrowski *et al.* 2015, 2017). Modulated Chl *a* fluorescence parameters are related to plant carbon assimilation, which mainly reflect the actual light energy utilization and distribution of PSII (Qiu *et al.* 2013). Prompt Chl fluorescence (OJIP curve) can reflect energy

and electron transfer process in thylakoid membranes, the activities of PSII donor and acceptor sides, and the redox changes of the electron transporter (Li *et al.* 2005, Kalaji *et al.* 2017). In addition, the modulated 820-nm reflection can be used to assess the functional state of PSI and analyze its coordination with PSII (Zhang *et al.* 2011, 2017). In *Brassica oleracea*, minimal fluorescence yield of the dark-adapted state (F_0), maximal fluorescence yield of the dark-adapted state (F_m), minimal fluorescence yield of the light-adapted state (F_0'), maximal quantum yield of PSII photochemistry (F_v/F_m), the efficiency of excitation capture of open PSII center (F_v'/F_m'), effective quantum yield of PSII photochemistry (Φ_{PSII}), photochemical quenching coefficient (q_P), nonphotochemical quenching coefficient (q_N), and electron transfer rate (ETR) in yellow-leaf cabbage (*Brassica oleracea*) mutant 'YL-1' were significantly lower than those of wild type (WT) plant (Yang *et al.* 2014). In *Pseudosasa japonica*, the electron transport chain from PSI to PSII was damaged, and the weakening of PSII activity resulted in immature chloroplast development, which might be the direct cause of the difference in leaf color of this species (Chen *et al.* 2018).

At present, there are few studies on leaf-color mutants combining two techniques (modulated fluorescence and prompt Chl fluorescence), and there is a lack of research on the PSI activity of leaf-color mutants. Our previous work showed that the natural yellowing mutant '*yl1*' of *Paeonia suffruticosa* Andr. cv. 'Wu Long Peng Sheng' is a 'chlorina' mutant with the low content of total Chl and Chl *b*, abnormal thylakoid structure, and reduced photosynthetic capacity (Chang *et al.* 2019). However, few studies have comprehensively focused on the functions of two photosystems in *yl1* mutant of tree peony. The *yl1* mutant could tolerate photooxidation damage in April, so we hypothesized that it had a corresponding adaptive strategy to photodamage. In this study, the physiological changes,

modulated Chl *a* fluorescence, prompt Chl fluorescence, and the modulated 820-nm reflection of *yl1* mutant and WT plants were compared in order to improve the further understanding of the theory of leaf color regulation of tree peony, and to provide a theoretical basis for the cultivation of leaf-viewed tree peony cultivars in the future.

Materials and methods

Plant materials: The *yl1* mutant and WT plants of *P. suffruticosa* Andr. cv. 'Wu Long Peng Sheng' were planted in the farm of Henan University of Science and Technology (34°33'N, 112°16'E). The soil in the experimental site is mainly cinnamon soil, with an average annual rainfall of 595 mm, an altitude of about 250 m, and an average annual temperature of 14.1°C (Chen and Yuan 2018). The water and fertilizer were managed under normal natural conditions in the open air. Tree peony was about 14 years old; six healthy *yl1* mutant and wild-type plants were used for experimental analysis in April 2019, respectively. On the basis of visual observation, the leaves of *yl1* mutants were fully extended and kept yellow in April. However, the yellow leaves of *yl1* mutants were susceptible to photooxidation stress under strong natural light, and even appeared photobleaching in May. Therefore, the leaves in April were used for analysis.

Antioxidant enzymes activities and soluble protein: The leaves (0.25 g) from the top of tree peony were ground in ice bath with 0.05 M phosphate acid buffer (pH 7.8) and centrifuged for 15 min at the speed of 3,000 rpm at 4°C, then the extract was stored in the refrigerator for the determination. The superoxide dismutase (SOD, EC 1.15.1.1) activity was assayed by the photochemical NBT method according to Li *et al.* (2018). SOD activity was measured in 3 ml of a reaction mixture containing 50 mM phosphate buffer (pH 7.8), 130 mM L-methionine, 100 mM EDTA, 750 μM NBT, 20 μM riboflavin, and 200 μl of the extract. The reaction was started with 20 μM riboflavin by exposing the cuvette to the fluorescent lamp group of 80 μmol(photon) $m^{-2} s^{-1}$ for 20 min. The reduction of NBT was determined at 560 nm (*722S*, *Lengguang*, Shanghai, China). One unit of SOD activity was defined to inhibit the photoreduction of NBT by 50%. The activity of catalase (CAT, EC 1.11.1.6) was assayed in a reaction mixture of 200 mM phosphate buffer (pH 7.8), 100 mM H_2O_2, and 200 μl of the extract (Wang *et al.* 2020). CAT activity was measured by tracking the consumption of H_2O_2 at 240 nm (*752S*, *Lengguang*, Shanghai, China) for 3 min. The soluble protein content (SP) was determined by the method as described by Bradford (1976). The extraction solution (1 ml) was mixed with 5.0 ml of *Coomassie Brilliant Blue G-250* reagent, and placed at room temperature for 2 min. Then the absorbance was measured at 595 nm by using a spectrophotometer (*722S*, *Lengguang*, Shanghai, China), the content of soluble protein was calculated according to the standard curve of bovine serum protein.

Soluble sugar content (SS): The soluble sugar content in the extract was determined by anthrone colorimetry according to Dong *et al.* (2019). The fresh leaves of 0.05 g were transferred to tubes with 8.0 ml of distilled water, and extracted twice in a boiling water for 30 min. The extract was filtered and the volume was adjusted to 25 mL with distilled water. The extraction solution (0.5 ml) was mixed with 1.5 mL of distilled water, 0.5 mL of ethyl anthrone acetate reagent, and 5 mL of concentrated sulfuric acid. Then the mixture in the test tube was placed in boiling water for 1 min. After cooling to room temperature, the absorbance was measured at 630 nm (*722S*, *Lengguang*, Shanghai, China). Finally, the glucose calibration curve was established for the accurate quantification of soluble sugar.

The content of proline (Pro): Proline content was determined according to the methods of Bates *et al.* (1973). A sample of 0.25 g of leaf was transferred into the tube with 5 ml of 3% sulfosalicylic acid solution, extracted in boiling water bath for 10 min; then the supernatant was filtered and cooled to room temperature. The extract (2 ml) was mixed with 2 ml of acetic acid and 2 ml of acid ninhydrin, and then the mixture was boiled for 30 min. When cooled to room temperature, 4 ml of toluene were added to the mixture. After shaking for 30 s, the upper liquid was centrifuged at 3,000 rpm for 5 min. The absorbance was determined at 520 nm (*722S*, *Lengguang*, Shanghai, China) using toluene for a blank. The content of Pro in the sample was calculated according to the standard curve of Pro.

Relative electrical conductivity (REC): REC was evaluated by the method of Johal *et al.* (2020). Leaf samples (0.1 g) were washed with distilled water and then placed in tubes with 10 ml of distilled water, kept at room temperature for 24 h. The initial electrical conductivity (C1) was measured with a conductivity meter (*DDS-11A*, *Yoke Instrument*, China). Then samples were boiled for 0.5 h at 100°C. After cooling, the electrical conductivity was measured again (C2). REC was calculated as the percentage ratio of (C2 – C1)/C2.

Malondialdehyde (MDA): MDA content was determined according to the method as described previously (Cai *et al.* 2019, Wu *et al.* 2021). The fresh leaves (0.25 g) were ground with 5 ml of 5% (w/v) trichloroacetic acid, and then centrifuged for 10 min at 3,000 rpm. The supernatant of 2 ml was added to 2 ml of 0.67% (w/v) TBA, boiled in water for 30 min, and centrifuged for 10 min at 3,000 rpm again after cooling. Then, the absorbance of the mixture was measured at 450, 532, and 600 nm (*722S*, *Lengguang*, Shanghai, China).

Hydrogen peroxide (H_2O_2) and superoxide radical ($O_2^{·-}$): H_2O_2 content was determined according to Velikova *et al.* (2000). Leaf samples (0.50 g) were ground in 5 ml of 1% trichloroacetic acid. The homogenates were centrifuged at 10,000 rpm for 10 min, then 0.20 ml of supernatant was mixed with 0.5 ml of 10 mM phosphate buffer (pH 7.0) and 1 ml of 1 M iodide potassium, then stored in the dark for 20 min. The mixture was centrifuged for 10 min at the speed of 10,000 rpm at 4°C, and the absorbance of

the supernatant was read at 390 nm (*752S*, *Lengguang*, Shanghai, China). The H_2O_2 content was quantified using a calibration curve obtained with different concentrations of H_2O_2.

The superoxide radical ($O_2^{\bullet-}$) concentration was measured according to the method as described previously (Liu *et al.* 2016b). A sample of 1.0 g of leaf was homogenized in 5 mL of 65 mM phosphate buffer (pH 7.8), filtered with four layers of gauze, and centrifuged at 1,000 rpm for 10 min, then the supernatant was diluted to 10 ml. Later, 2 mL of extract was added to 1.5 mL of 65 mM phosphate buffer (pH 7.8) and 0.5 mL of 10 mM hydroxylamine hydrochloride, the mixture was kept in a water bath for 20 min at 25°C. Two ml of the above mixture was added to a test tube containing 2 ml of 7 mM P-sulfanilic acid and 2 mL of 7 mM α-naphthylamine, then incubated for 30 min at 30°C. Finally, $O_2^{\bullet-}$ content was determined by measuring the absorbance at 530 nm (*722S*, *Lengguang*, Shanghai, China).

Chl fluorescence: The Chl fluorescence parameters of the 3–4th completely expanded leaves from the apex of tree peony were measured at 9:00–12:00 h in the morning by using a modulated fluorometer (*Mini-PAM*, *Walz*, Germany). The acting light, the flash, and the saturation pulse were set to 1,000; 0.9, and > 4,000 μmol(photon) $m^{-2} s^{-1}$, respectively. A dark treatment was conducted for 30 min, then F_0, F_m, F_v/F_m, F_0', maximum fluorescence of the light-adapted state (F_m'), F_v'/F_m', Φ_{PSII}, q_P, and ETR were then recorded according to the method of Genty *et al.* (1989).

The fraction of absorbed light energy was calculated according to the method of Demmig-Adams *et al.* (1996). The fraction of absorbed light energy used for PSII photochemistry (P) was calculated as $P = F_v'/F_m' \times q_P$, the light energy utilized in thermal dissipation (D) was estimated as $D = 1 - F_v'/F_m'$, the absorbed energy that is in excess of that which can be thermally dissipated or used in photochemistry (E) was calculated from $E = F_v'/F_m' \times (1 - q_P)$.

The Chl *a* fluorescence transient (OJIP) and modulated 820-nm reflection transients: The 3–4th leaves from the top in tree peony were used for determination at 9:00–11:00 h on a sunny day. The leaves were dark-adapted for at least 30 min, and then the prompt Chl fluorescence induction kinetics curve (OJIP) and modulated 820-nm reflection were simultaneously measured by *M-PEA* (*Hansatech*, Norfolk, UK). The OJIP curve was induced by saturated pulsed light with a light intensity of 3,000 μmol(photon) $m^{-2} s^{-1}$. The fluorescence signal was recorded from 10 μs to 2 s. The parameters of Chl *a* fluorescence transient (Appendix) were calculated by the JIP-test according to Strasser *et al.* (2010). The relative variable fluorescence was calculated as $V_t = (F_t - F_0)/(F_m - F_0)$, $\triangle V_t = V_{t\,yll} - V_{t\,WT}$, according to the method of Li *et al.* (2010a).

The modulated 820-nm reflection transients in the leaves were induced by 250 μmol(photon) $m^{-2} s^{-1}$ far-red light, and the measurement was performed on a clear day from 9:00 to 11:00 h. The 820-nm modulated reflection

was expressed by MR/MR_0; MR_0 is the light reflectance value of the initial illumination (taken from 0.7 ms in this study, the first credible MR measurement value), and MR is the light reflectance value of 820 nm during the illumination process (Liu *et al.* 2017). In this paper, the maximum redox activity of PSI was reflected by $\triangle I/I_0$, where I_0 is the average value of the 820-nm transmission signal between 0.4 and 10 ms and I_m is the average of the 820-nm transmission signal between 3 and 10 s, while the following formula was used to calculate $\triangle I/I_0 = (I_0 - I_m)/I_0$, the coordination between PSI and PSII ($\Phi_{(PSI/PSII)}$), $\Phi_{(PSI/PSII)} = (\triangle I/I_0)/\Psi_0$ (Strasser *et al.* 2004, Zhang *et al.* 2011).

Statistical analysis: All physiological parameters were measured with at least three biological replicates, while other parameters were measured with six biological replicates. The resulting data were analyzed by unpaired *t*-test in *SPSS 13.0* (*SPSS Inc.*, Chicago, IL, USA) for comparison at $P<0.05$ level.

Results

Differences in biochemical indexes: The activities of SOD and CAT, the contents of soluble protein, proline, MDA, $O_2^{\bullet-}$ and REC in yellow leaves of *yl1* mutant were significantly higher than those of WT plants (Table 1), while the soluble sugar content decreased greatly. The H_2O_2 content in *yl1* mutant was higher than that in WT plant, but there were no significant differences between them.

Photochemical efficiency: The parameters of F_0, F_m, F_0', F_m', F_v/F_m, F_v'/F_m', Φ_{PSII}, and ETR all significantly decreased in *yl1* mutant compared with those of the WT (Table 2), only q_P showed no significant differences between two different leaf types.

Light absorption and distribution: The light energy absorbed by PSII can be divided into three parts, including the photochemical reaction (P), the thermal dissipation (D), and excess absorbed light energy (E). The fraction of P and E in *yl1* mutant was greatly lower than those of WT plant (Fig. 1), while the fraction of D of *yl1* mutant was significantly higher than that of WT.

The changes of prompt Chl fluorescence: The appearance of K-band is widely used as specific indicator of the damage of the oxygen-evolving complex (OEC) at the PSII donor side, while J- and I-band mainly reflect the activity of the PSII acceptor side (Kalaji *et al.* 2014). The relative fluorescence between the O- and P-steps were normalized (V_t) and expressed as the kinetic differences ($\triangle V_t$) to analyze the changes between *yl1* mutant and WT plants (Fig. 2). All Chl *a* fluorescence transient curves (V_t) displayed a typical polyphasic rise with the basic steps of OJIP. OJIP curves from *yl1* mutants showed a more obvious rise at the K-, J-, and I-step than those in WT plants (Fig. 2*A*). The *yl1* mutant showed positive $\triangle K$-, $\triangle J$-, and $\triangle I$-bands around 300 μs, 2 ms, and 30 ms in respect

Table 1. Biochemical parameters of the wild type and *yl1* mutant. WT – wild type; *yl1* – *yl1* mutant. *$P<0.05$ using *t*-test. CAT – catalase; MDA – malondialdehyde; Pro – proline; REC – relative electrical conductivity; SOD – superoxide dismutase; SP – soluble protein; SS – soluble sugar.

Type	SOD [U g^{-1} min^{-1}]	CAT [U g^{-1} min^{-1}]	SP [mg g^{-1}]	SS [mg g^{-1}]	Pro [µg ml^{-1}]	REC [%]	MDA [nmol g^{-1}]	H$_2$O$_2$ [µmol g^{-1}]	O$_2^{\cdot-}$ [µg g^{-1}]
WT	243.07 ± 17.00	23.81 ± 5.98	2.12 ± 0.11	15.04 ± 0.93*	52.52 ± 5.67	42.33 ± 3.52	10.18 ± 2.12	63.91 ± 5.04	5.66 ± 1.91
yl1	283.22 ± 4.18*	36.66 ± 6.84*	2.67 ± 0.08*	7.05 ± 0.83	77.21 ± 4.73*	52.61 ± 2.15*	15.26 ± 2.36*	70.67 ± 1.07	11.87 ± 1.17*

Table 2. Photochemical parameters of wild type and *yl1* mutant. WT – wild type; *yl1* – *yl1* mutant. *$P<0.05$ using *t*-test. ETR – electron transfer rate; F$_0$' – minimal fluorescence yield of the light-adapted state; F$_m$ – maximal fluorescence yield of the dark-adapted state; F$_m$' – maximal fluorescence yield of the light-adapted state; F$_v$/F$_m$ – maximal quantum yield of PSII photochemistry; F$_v$'/F$_m$' – the efficiency of excitation capture of open PSII center; q$_P$ – photochemical quenching coefficient; Φ_{PSII} – effective quantum yield of PSII photochemistry.

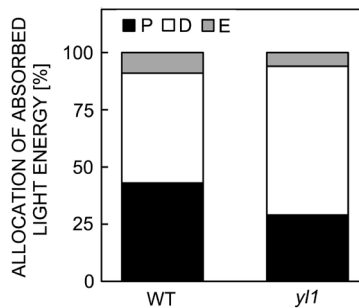| Type	F$_0$	F$_m$	F$_0$'	F$_m$'	F$_v$/F$_m$	F$_v$'/F$_m$'	Φ_{PSII}	q$_P$	ETR
WT	346.75 ± 39.55*	1,318.25 ± 212.98*	244.13 ± 14.05*	513.67 ± 60.30*	0.73 ± 0.03*	0.52 ± 0.05*	0.43 ± 0.03*	0.82 ± 0.03	34.05 ± 2.50*
yl1	233.00 ± 4.24	428.00 ± 31.11	177.67 ± 0.47	270.33 ± 16.97	0.45 ± 0.05	0.35 ± 0.04	0.29 ± 0.02	0.84 ± 0.05	23.02 ± 1.41

Fig. 1. Allocation of absorbed light energy in wild type and *yl1* mutant. P – the light energy used for PSII photochemistry; D – the light energy utilized in thermal dissipation; E – the absorbed energy that is in excess of that which can be thermally dissipated or used in photochemistry. WT – wild type; *yl1* – *yl1* mutant.

Fig. 2. Changes in the shape of the chlorophyll *a* fluorescence transient curves of wild type and *yl1* mutant. Chl *a* fluorescence transients were normalized between F$_0$ to F$_P$: V$_t$ = (F$_t$ – F$_0$)/(F$_m$ – F$_0$) (*A*); ΔV$_t$ was the difference of V$_t$ between *yl1* mutant and wild type plant in tree peony: ΔV$_t$ = V$_{t\ yl1}$ – V$_{t\ WT}$ (*B*). WT – wild type; *yl1* – *yl1* mutant.

to WT plant (Fig. 2*B*). In order to quantify changes in the K-, J-, and I-steps in the OJIP curves, the normalized relative variable fluorescence at the K-step (W$_K$), and the relative variable fluorescence at the J-step (V$_J$) and I-step (V$_I$) were calculated (Fig. 3). The value of W$_K$, V$_J$, and V$_I$ in *yl1* mutants all increased markedly compared to those of WT plants. The increase of V$_J$ was more obvious in *yl1* mutants than that in W$_K$ and V$_I$, while the increase of W$_K$ was greater than that in V$_I$.

The parameters of M$_0$, Ψ_0, φE$_0$, and S$_M$ mainly reflect the changes of PSII acceptor side (Li *et al.* 2005). The value of M$_0$ in *yl1* mutant was significantly higher than that of WT plant (Table 3), while the values of Ψ_0 and φE$_0$ of *yl1* mutant were greatly lower than those of WT plant. The value of S$_m$ in *yl1* mutant was also lower than that of the WT plant.

The values of ABS/RC, TR$_0$/RC, and DI$_0$/RC in *yl1* mutant were significantly higher than those of WT plant (Fig. 4), while ET$_0$/RC was much lower in the *yl1* mutant than that of WT plant. As shown in Fig. 4, the values of RC/CS$_0$, ABS/CS$_0$, TR$_0$/CS$_0$, ET$_0$/CS$_0$, and PI$_{ABS}$ of *yl1*

mutant all significantly decreased than those of WT plant. The value of DI$_0$/CS$_0$ of *yl1* mutant was lower than that of WT but the difference was not significant.

The changes in PSI: The 820-nm curve of *yl1* mutant changed significantly compared with the control, and its lowest point of its MR/MR$_0$ greatly increased (Fig. 5). The ΔI/I$_0$ of *yl1* mutant was significantly lower than that of WT plant.

Fig. 3. The changes of relative variable fluorescence of wild type and *yl1* mutant. W_K – normalized relative variable fluorescence at the K-step; V_J and V_I – relative variable fluorescence at the J- and I-step; WT – wild type; *yl1* – *yl1* mutant. * – significant differences between WT and *yl1* mutant ($P<0.05$).
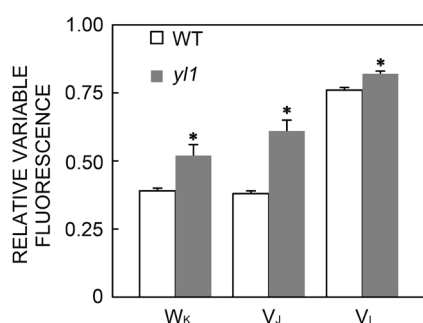
Table 3. Changes of chlorophyll *a* fluorescence transient of wild type and *yl1* mutant. WT – wild type; *yl1* – *yl1* mutant. *$P<0.05$ using *t*-test. M_0 – the initial slope of the relative variable fluorescence of the relative rate at which Q_A is reduced; S_m – normalized total complementary area above the OJIP transient; φE_0 – quantum yield for electron transport (at t = 0); Ψ_0 – probability that a trapped exciton moves an electron into the electron transport chain beyond Q_A^- (at t = 0).

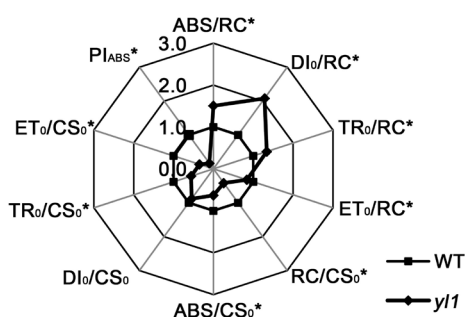| Type	M_0	Ψ_0	φE_0	S_m
WT	0.59 ± 0.01	$0.62 \pm 0.01^*$	$0.48 \pm 0.01^*$	28.24 ± 0.25
yl1	$1.28 \pm 0.17^*$	0.39 ± 0.04	0.27 ± 0.01	24.29 ± 2.00

Fig. 4. The energy fluxes and performance index (PI_{ABS}) of wild type and *yl1* mutant. WT – wild type; *yl1* – *yl1* mutant. * – significant differences between WT and *yl1* mutant ($P<0.05$); all the values in *yl1* mutant were expressed relative to WT plants (set as 1). ABS/CS_0 – absorption flux per CS (at t = 0); ABS/RC – absorption flux per reaction center (RC); DI_0/CS_0 – dissipated energy flux per CS (at t = 0); DI_0/RC – dissipated energy flux per RC (at t = 0); ET_0/CS_0 – electron transport flux per CS (at t = 0); ET_0/RC – electron transport flux per RC (at t = 0); RC/CS_0 – density of RCs per excited cross-section (CS) (at t = 0); TR_0/CS_0 – trapped energy flux per CS (at t = 0); TR_0/RC – trapped energy flux per RC (at t = 0).

The ratio of $\triangle I/I_0$ to Ψ_0 can represent the coordination between PSI and PSII (Li *et al*. 2010b). The value of

$\Phi_{(PSI/PSII)}$ of the *yl1* mutant was significantly lower than that of WT plant (Fig. 6), which indicated that the coordination between two photosystems of *yl1* mutant was reduced.

Discussion

Excessive ROS generation can promote phospholipid peroxidation, destroy cell membrane, and increase the penetration of intracellular electrolytes. MDA content is considered to be an important indicator of lipid peroxidation level. Leaf-color mutants were susceptible to photooxidative stress and some showed severe membrane lipid peroxidation and electrolyte leakage (Li 2016). In this study, the significant increase of MDA content and REC of *yl1* mutant suggested that it suffered severe photooxidation of the cell membrane and electrolyte leakage, which was also confirmed by the obvious increase of H_2O_2 and $O_2^{\cdot-}$ contents in the *yl1* mutant. In addition, ROS can directly destroy the PSII reaction center (Krieger-Liszkay *et al*. 2011), hinder the repair of PSII, and aggravate the photoinhibition damage by inhibiting the synthesis of D1 protein in the photosystem (Takahashi and Murata 2008). Our results confirmed these findings, as *yl1* mutant plant showed a lower RC/CS_0 and F_v/F_m.

In order to resist oxidative damage by ROS, the antioxidant enzymes can catalyze ROS detoxification (Labudda *et al*. 2020). The *yl1* mutant could reduce the damage caused by ROS by increasing activities of SOD and CAT and enhance the ability of osmotic regulation by increasing the contents of soluble protein and Pro. This study was consistent with previous studies on leaf color mutants of melon (*Cucumis melo*) (Lai *et al*. 2018) and cucumber (*Cucumis sativus*) (Li *et al*. 2015). It is well known that SOD catalyzes the conversion of $O_2^{\cdot-}$ to H_2O_2, and H_2O_2 can be eliminated by CAT (Labudda *et al*. 2020). The yellow leaves of *yl1* mutant could improve SOD and CAT activities to scavenge ROS and protect the photosystems; similar studies also appeared in the albino tissue of Hibotan-nishiki cactus (*Gymnocalycium mihanovichii*) (Deng 2009). In this study, the increase of $O_2^{\cdot-}$ content was higher than that of H_2O_2 in the *yl1* mutant, which was similar to the results of the rice (*Oryza sativa*) zebra-leaf mutant *l139* (Guo 2020); such results might be observed because the increase of CAT activity was higher than that of SOD activity.

Soluble sugar is one of the main storage substances of the energy metabolism in plants. In this study, the decrease of soluble sugar content in *yl1* mutant might occur due to the decline of PSII and PSI functions and lower photosynthetic rate (Chang *et al*. 2019). This study was consistent with that of rice (*Oryza sativa*) yellow-leaf mutant (Hu 2017) and yellow-leaf mutant *rgm* (1-20YY) in common wheat (*Triticum aestivum*) (Liu *et al*. 2016a). Soluble proteins are important osmotic adjustment substances and nutrients, most of which are enzymes involved in metabolism (Li 2016). Previous studies have shown that the soluble sugar contents of cucumber (*Cucumis sativus*) and anthurium (*Anthurium andraeanum*) leaf-color mutants were lower than those of the control, but the soluble protein contents were higher than those of the control (Chen 2009, Li 2016),
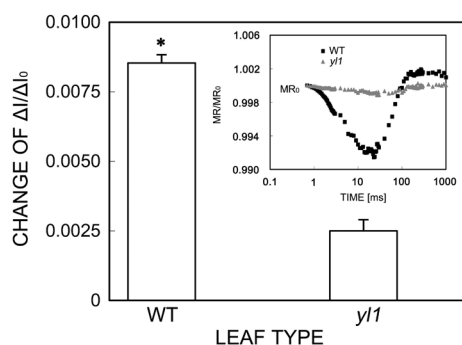
Fig. 5. The changes of modulated 820-nm reflection curves and maximum PSI redox activity of the wild type and *yl1* mutant. WT – wild type; MR_0 – the light reflectance value of the initial illumination; MR – the light reflectance value of 820 nm during the illumination process; WT – wild type; *yl1* – *yl1* mutant. * – significant differences between WT and *yl1* mutant ($P<0.05$).
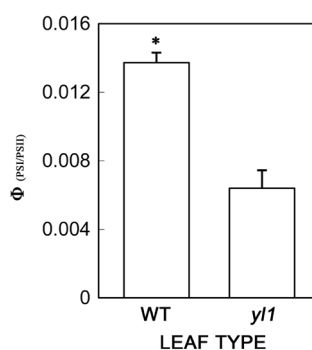

Fig. 6. Changes of coordination between PSI and PSII ($\Phi_{(PSI/PSII)}$) of the wild type and *yl1* mutant. WT – wild type; *yl1* – *yl1* mutant. * – significant differences between WT and *yl1* mutant ($P<0.05$).

which was similar to this study. It was speculated that the specific expression of some genes in the leaves of the mutants increased, which led to an increase of the soluble protein content (Li 2016). The increase of Pro content in *yl1* mutant could maintain cell turgor, prevent electrolyte leakage, and reduce the damage by ROS (Rastogi *et al.* 2020), which was consistent with previous studies on the light-green leaf mutant in *Sorghum bicolor* (Zhang *et al.* 2014).

The decrease of F_0, F_m, F_0', and F_m' in *yl1* mutant showed a reduction of light energy capture efficiency and utilization in PSII reaction center. The lower values of F_v/F_m, F_v'/F_m', Φ_{PSII}, and ETR of *yl1* mutant indicated that the light energy-utilization efficiency decreased in *yl1* mutant (Xiao *et al.* 2013, Yang *et al.* 2014), which was consistent with the photosynthetic rate of *yl1* mutant measured previously (Chang *et al.* 2019). There was no significant difference in q_P between *yl1* mutant and WT, which might imply that the reduction of Chl content did not necessarily have a significant effect on photochemical quenching. This study was consistent with leaf-color mutants in *Brassica rapa* (Liu *et al.* 2014) and *Pseudosasa japonica* (Chen *et al.* 2018).

The fraction of P significantly decreased which could reduce the load of PSII reaction center. The increase of the proportion of D implied the excess light energy could be dissipated by thermal dissipation, thus protecting photosynthetic apparatus (Yang *et al.* 2009). The significant reduction of E could not only reduce the excitation pressure of PSII and the formation of superoxide radical but also reduce the reversible deactivation or destruction of the photosystems (Hu *et al.* 2005). The changes of D and E might indicate that *yl1* mutant had the ability to avoid oxygen stress.

The K-steps on the OJIP curve raised greatly in the *yl1* mutant, which indicated that the OEC on the donor side of PSII had been severely damaged (Parmoon *et al.* 2019). The increase of J-steps showed that the acceptor side of *yl1* mutant was also injured; the increase of phase J was higher than that of phase K, indicating that the damage on the acceptor side was significantly higher than that of donor side.

In this study, the lower value of φE_0 in the *yl1* mutant indicated that the relative electron transfer ability decreased. The increase of M_0 and V_J indicated that the reduction rate of Q_A was accelerated, the electron transfer from PSII acceptor side Q_A to secondary quinone receptor (Q_B) was blocked, resulting in the accumulation of Q_A^- in *yl1* mutant (Li *et al.* 2005). The increase in V_I steps on the OJIP curve in *yl1* mutant indicated that the electron transfer from Q_B to the downstream was further blocked. The decrease in S_m indicated that the PQ pool of the electron acceptor of PSII was reduced, and the number of the electron transporters accepted by the acceptor side of PSII was reduced, which led to a decrease in φE_0 and Ψ_0.

A significant increase of ABC/RC and TR_0/RC reflected that the *yl1* mutant could increase the ability of light absorption and capture of a single reaction center and promote the efficiency improvement of the remaining active reaction centers, thus making up for the deficiency of *yl1* mutant in the number of reaction centers, which might be a compensation mechanism. The decline in ET_0/RC of yellow leaves showed that the quantum share of yellow leaves used for electron transport was reduced, which was in agreement with the significant decrease of ETR. The ABS/RC and TR_0/RC in *yl1* mutant increased greatly, while the ET_0/RC decreased significantly, which indicated that the weakening of the dynamics of electron transport from OEC to PSII, and a large amount of electrons accumulated at the Q_A side (Souza *et al.* 2019). A marked increase in DI_0/RC of *yl1* mutant indicated a loss of absorbed excitation energy as heat and fluorescence rather than photochemistry, which was consistent with the higher proportion of thermal dissipation (D).

The significant decrease of RC/CS_0, ABS/CS_0, TR/CS_0, and ET/CS_0 suggested that there was a large amount of energy accumulation in *yl1* mutant, which would increase ROS content and damage OEC (Li *et al.* 2009).

Although the utilization capacity of light energy per reaction center increased, the improvement of the efficiency per reaction center could not compensate for the decrease of the number of active centers per excited cross-section (RC/CS_0), which led to the decrease in the

utilization rate of light energy per excited cross-section (Li *et al.* 2009), and finally resulted in a significant decline in PI_{ABS} of *yl1* mutant. In this study, the decrease of φE_0 and the increase of V_J, V_I, and M_0 indicated that the PSII reaction center of *yl1* mutant was inactivated and electron transfer of PSII was blocked, which made yellow leaves of *yl1* mutant more susceptible to photoinhibition, resulting in a significant decrease of F_v/F_m.

MR/MR_0 represents the redox state of P_{700} and plastocyanin (PC) (Sun *et al.* 2017). The increase in the lowest point of MR/MR_0 of the *yl1* mutant showed that the oxidation rate of P_{700} and PC slowed down, which indicated that the amount of electrons transferred to P_{700}^+ decreased. The parameter of $\Delta I/I_0$ represents the performance of PSI. The significant decrease in $\Delta I/I_0$ of *yl1* mutant showed that the function of PSI was weakened. The changes of $\Delta I/I_0$ and F_v/F_m can be used to estimate the photoinhibition of PSI and PSII, respectively (Guo *et al.* 2018). The reduction of $\Delta I/I_0$ and F_v/F_M indicated that PSI and PSII of *yl1* mutant were photoinhibited in different degrees. F_0 can be regarded as a reliable indicator of PSI/PSII ratio (Pfündel *et al.* 2013). A significant decrease in F_0 indicated a reduction of PSI/PSII ratio in the *yl1* mutant, which would result in an imbalance between the two photosystems (Brestic *et al.* 2015). The reduction in the activities of PSI and PSII and the imbalance of PSI/PSII in the *yl1* mutant would reduce the efficiency of the electron transport chain after Q_A, block the electron flow from PSI, aggravate photoinhibition, and produce a large amount of ROS (Liu *et al.* 2018), which was confirmed by the increase of ROS in *yl1* mutant.

In summary, the obvious rise of the K-, J-, and I-steps of the OJIP curves indicated that OEC of *yl1* mutant was damaged and the electron transfer of PSII was blocked, which further affected the electron transfer to PSI. Due to the different degree of photoinhibition of these two photosystems, the activities of PSI and PSII decreased, accompanied by an imbalance of PSI/PSII, which ultimately led to the decline of PI_{ABS} of *yl1* mutant. As the electron transfer from PSII to PSI was blocked, *yl1* mutant produced a lot of ROS, which led to the increase of REC and MDA. The *yl1* mutant could reduce the damage of ROS by increasing the activity of antioxidant enzymes and the contents of some osmotic adjustment substances and reduce the damage caused by excessive light energy by increasing the proportion of heat dissipation.

References

Bates L.S., Waldren R.P., Teare I.D.: Rapid determination of free proline for water-stress studies. – Plant Soil **39**: 205-207, 1973.

Bradford M.M.: A rapid and sensitive method for the quantitation of microgram quantities of protein utilizing the principle of protein-dye binding. – Anal. Biochem. **72**: 248-254, 1976.

Brestic M., Zivcak M., Kunderlikova K. *et al.*: Low PSI content limits the photoprotection of PSI and PSII in early growth stages of chlorophyll *b*-deficient wheat mutant lines. – Photosynth. Res. **125**: 151-166, 2015.

Cai H., Xie P., Zeng W. *et al.*: Root-specific expression of rice *OsHMA3* reduces shoot cadmium accumulation in transgenic tobacco. – Mol. Breeding **39**: 49, 2019.

Chai C., Fang J., Liu Y. *et al.*: *ZEBRA2*, encoding a carotenoid isomerase, is involved in photoprotection in rice. – Plant Mol. Biol. **75**: 211-221, 2011.

Chang Q.S., Zhang L.X., Hou X.G. *et al.*: The anatomical, physiological and molecular analysis of a chlorophyll-deficient mutant in tree peony (*Paeonia suffruticosa*). – Photosynthetica **57**: 724-730, 2019.

Chen K.Y., Li C.N., Cheng M.M. *et al.*: [Chloroplast ultrastructure and chlorophyll fluorescence characteristics of three cultivars of *Pseudosasa japonica*.] – Chin. Bull. Bot. **53**: 509-518, 2018. [In Chinese]

Chen L., Yuan Q.Z.: [Study on Luoyang tourism climate comfort based on entropy method.] – J. Luoyang Normal Univ. **37**: 20-25, 2018. [In Chinese]

Chen X.X.: [Formative mechanism and maintenance characteristics of leaf color chimera and mutants of *Anthurium andreaeanum* 'Sonate'.] Master Thesis. Nanjing Agricultural University, Nanjing 2009. [In Chinese]

Chu J.T.: [Study on leaf color variation mechanism of a new cultivar 'Golden qilu' in *Acer buergerianum* Miq.] Master Thesis. Shandong Agricultural University, Taian 2020. [In Chinese]

Dąbrowski P., Kalaji M.H., Baczewska A.H. *et al.*: Delayed chlorophyll *a* fluorescence, MR 820, and gas exchange changes in perennial ryegrass under salt stress. – J. Lumin. **183**: 322-333, 2017.

Dąbrowski P., Pawluśkiewicz B., Baczewska A.H. *et al.*: Chlorophyll *a* fluorescence of perennial ryegrass (*Lolium perenne* L.) varieties under long term exposure to shade. – Zemdirbyste **102**: 305-312, 2015.

Demmig-Adams B., Adams III W.W., Barker D.H. *et al.*: Using chlorophyll fluorescence to assess the fraction of absorbed light allocated to thermal dissipation of excess excitation. – Physiol. Plantarum **98**: 253-264, 1996.

Deng B.L.: [Albino plant and higher endogenous reactive oxygen species toxicity.] Master Thesis. Lanzhou University, Lanzhou 2009. [In Chinese]

Dong F., Wang C., Sun X. *et al.*: Sugar metabolic changes in protein expression associated with different light quality combinations in tomato fruit. – Plant Growth Regul. **88**: 267-282, 2019.

Du Q., Wang N., Zhao X.H. *et al.*: [Effects of potassium deficiency on photosynthesis and performance of photosystem II in maize seedling stage.] – J. Nucl. Agric. Sci. **33**: 592-599, 2019. [In Chinese]

Genty B., Briantais J.M., Baker N.R.: The relationship between the quantum yield of photosynthetic electron transport and quenching of chlorophyll fluorescence. – BBA-Gen. Subjects **990**: 87-92, 1989.

Guo N.H.: [Gene mapping and physiological characteristics analysis of a zebra leaf mutant *l139* in rice.] Master Thesis. Shenyang Agricultural University, Shenyang 2020. [In Chinese]

Guo Y.Y., Tian S.S., Liu S.S. *et al.*: Energy dissipation and antioxidant enzyme system protect photosystem II of sweet sorghum under drought stress. – Photosynthetica **56**: 861-872, 2018.

Hu W.H., Xiao Y.A., Yu J.Q. *et al.*: [Effects of different light intensity after low night temperature stress on PSII functions and absorbed light allocation in leaves of *Ficus macrocarpa*.] – Bull. Bot. Res. **25**: 159-162, 2005. [In Chinese]

Hu Z.: [Gene cloning and functional analysis of *yl1* conferring the leaf color through characterizing the rice *yl1* mutant.] Master Thesis. Yangzhou university, Yangzhou 2017. [In Chinese]

Johal N., Kaur J., Grewal S.K. *et al.*: Physiological and bio-

chemical responses of chickpea accessions at reproductive stage under receding moisture conditions. – Agr. Res. **9**: 554-567, 2020.

Kalaji H.M., Schansker G., Brestic M. *et al.*: Frequently asked questions about chlorophyll fluorescence, the sequel. – Photosynth. Res. **132**: 13-66, 2017.

Kalaji H.M., Schansker G., Ladle R.J. *et al.*: Frequently asked questions about *in vivo* chlorophyll fluorescence: Practical issues. – Photosynth. Res. **122**: 121-158, 2014.

Krieger-Liszkay A., Kós P.B., Hideg E.: Superoxide anion radicals generated by methylviologen in photosystem I damage photosystem II. – Physiol. Plantarum **142**: 17-25, 2011.

Labudda M., Tokarz K., Tokarz B. *et al.*: Reactive oxygen species metabolism and photosynthetic performance in leaves of *Hordeum vulgare* plants co-infested with *Heterodera filipjevi* and *Aceria tosichella*. – Plant Cell Rep. **39**: 1719-1741, 2020.

Lai Y., Fu Q.S., Lv J.C. *et al.*: [Analysis of physiological characteristics and chloroplast ultrastructure of a new leaf color mutant in melon.] – J. Sichuan Agric. Univ. **36**: 372-379, 2018. [In Chinese]

Li G., Gao H.Y., Liu P. *et al.*: [Effects of nitrogen fertilization on photosynthetic performance in maize leaf at grain filling stage.] – Plant Nutr. Fert. Sci. **16**: 536-542, 2010b. [In Chinese]

Li G., Gao H.Y., Zhao B. *et al.*: [Effects of drought stress on activity of photosystems in leaves of maize at grain filling stage.] – Acta Agron. Sin. **35**: 1916-1922, 2009. [In Chinese]

Li P.M., Gao H.Y., Strasser R.J.: [Application of the fast chlorophyll fluorescence induction dynamics analysis in photosynthesis study.] – J. Plant Physiol. Mol. Biol. **31**: 559-566, 2005. [In Chinese]

Li Q., Chen L.S., Jiang H.X. *et al.*: Effects of manganese-excess on CO_2 assimilation, ribulose-1,5-bisphosphate carboxylase/ oxygenase, carbohydrates and photosynthetic electron transport of leaves, and antioxidant systems of leaves and roots in *Citrus grandis* seedlings. – BMC Plant Biol. **10**: 42, 2010a.

Li W.Q., Gao B., Yang J. *et al.*: [Physiological characteristic analysis of a new leaf color yellow mutant in cucumber.] – Acta Agric. Bor.-Occident. Sin. **24**: 98-103, 2015. [In Chinese]

Li X., Brestic M., Tan D.X. *et al.*: Melatonin alleviates low PS I-limited carbon assimilation under elevated CO_2 and enhances the cold tolerance of offspring in chlorophyll *b*-deficient mutant wheat. – J. Pineal Res. **64**: e12453, 2018.

Li Y.: [Physiological characteristics and genetic analysis of leaf color mutant in cucumber.] Master Thesis. Sichuan Agricultural University, Chendu 2016. [In Chinese]

Liu A.R., Wang M.M., Liu D.L. *et al.*: Arbuscular mycorrhizal fungus alleviates chilling stress by boosting redox poise and antioxidant potential of tomato seedlings. – J. Plant Growth Regul. **35**: 109-120, 2016b.

Liu C., Duan Y., An X. *et al.*: [Comparison of main physiological characteristics, chloroplast morphology and ultra-structure of the yellow-green wheat (*Triticum aestivum*) near-isogenic lines.] – J. Agric. Biotech. **24**: 806-814, 2016a. [In Chinese]

Liu J., Yang Y.H., Hao Y.C. *et al.*: [Effects of photosynthetic electron transport chain of maize leaves under drought stress and re-watering.] – Plant Physiol. J. **53**: 1877-1884, 2017. [In Chinese]

Liu M.J., Sui X.Q., An S.Z.: [The effect of dehydration on *Cynodon dactylon* L. leaf photosynthetic apparatus.] – Acta Agr. Sin. **26**: 441-446, 2018. [In Chinese]

Liu M.Y., Lu Y., Zhao J.J. *et al.*: [HRM identification and chlorophyll fluorescence characteristics on leaf color mutants in chinese cabbage.] – Acta Hortic. Sin. **41**: 2215-2224, 2014.

[In Chinese]

Lv D.H.: [Study on photosynthetic, physiological and biochemical characteristics in leaf color mutants of rice (*Oryza sativa* L.).] Master Thesis. Southwest University, Chongqing 2010. [In Chinese]

Parmoon G., Ebadi A., Jahanbakhsh S. *et al.*: Assessing photosynthetic performance of fennel (*Foeniculum vulgare* Mill) influenced by plant growth regulators and drought stress imposed at vegetative and reproductive stages. – Ital. J. Agron. **14**: 93-100, 2019.

Pfündel E.E., Klughammer C., Meister A., Cerovic Z.G.: Deriving fluorometer-specific values of relative PSI fluorescence intensity from quenching of F_O fluorescence in leaves of *Arabidopsis thaliana* and *Zea mays*. – Photosynth. Res. **114**: 189-206, 2013.

Qiu N.W., Zhou F., Wang Y. *et al.*: [Comparison on characteristics of the fast chlorophyll fluorescence induction kinetics between *Pinus* species and *Populus* species.] – Sci. Silva. Sin. **49**: 136-143, 2013. [In Chinese]

Rastogi A., Kovar M., He X. *et al.*: JIP-test as a tool to identify salinity tolerance in sweet sorghum genotypes. – Photosynthetica **58**: 518-528, 2020.

Ru G.X., Liu X.N., Zhu X.H. *et al.*: [Physiological characteristic analysis of etiolation mutant in *Paulownia fortnnei*.] – J. Nanjing Forest. Univ. **60**: 181-185, 2017. [In Chinese]

Souza A.F.C, Martins J.P.R., Gontijo A.B.P.L., Falqueto A.R.: Selenium improves the transport dynamics and energy conservation of the photosynthetic apparatus of *in vitro* grown *Billbergia zebrina* (Bromeliaceae). – Photosynthetica **57**: 931-941, 2019.

Strasser R.J., Tsimilli-Michael M., Qiang S., Goltsev V.: Simultaneous *in vivo* recording of prompt and delayed fluorescence and 820-nm reflection changes during drying and after rehydration of the resurrection plant *Haberlea rhodopensis*. – BBA-Bioenergetics **1797**: 1313-1326, 2010.

Strasser R.J., Tsimilli-Michael M., Srivastava A.: Analysis of the chlorophyll *a* fluorescence transient. – In: Papageorgiou G.C., Govindjee (ed.): Chlorophyll *a* Fluorescence: A Signature of Photosynthesis. Advances in Photosynthesis and Respiration. Pp. 321-362. Springer, Dordrecht 2004.

Sun Y.P., Liu J., Cao R.X. *et al.*: Effects of 5-aminolevulinic acid treatment on photosynthesis of strawberry. – Photosynthetica **55**: 276-284, 2017.

Takahashi S., Murata N.: How do environmental stresses accelerate photoinhibition? – Trends Plant Sci. **13**: 178-182, 2008.

Velikova V., Yordanov I., Edreva A.: Oxidative stress and some antioxidant systems in acid rain-treated bean plants: protective role of exogenous polyamines. – Plant Sci. **151**: 59-66, 2000.

Wang N., Tian Y.W., Chen H.: Seed dormancy and germination response of *Aegilops tauschii* to exogenous application of GA_3 and warm water. – Int. J. Agric. Biol. **24**: 885-890, 2020.

Wang Y., Zheng W., Zheng W.J. *et al.*: Physiological and transcriptomic analyses of a yellow-green mutant with high photosynthetic efficiency in wheat (*Triticum aestivum* L.). – Funct. Integr. Genomic. **8**: 175-194, 2018.

Wu M.J., Yan Y.R., Wang Y.Q. *et al.*: Arbuscular mycorrhizal fungi for vegetable (VT) enhance resistance to *Rhizoctonia solani* in watermelon by alleviating oxidative stress. – Biol. Control **152**: 104433, 2021.

Xiao H.G., Yang H.W., Rao Y. *et al.*: [Analysis of chloroplast ultrastructure, stomatal characteristic parameters and photosynthetic characteristics of chlorophyll-reduced mutant in *Brassica napus* L.] – Sci. Agr. Sin. **46**: 715-727, 2013. [In Chinese]

Yang C., Zhang Y.Y., Fang Z.Y. *et al.*: [Photosynthetic

physiological characteristics and chloroplast ultrastructure of yellow leaf mutant *YL-1* in cabbage.] – Acta Hortic. Sin. **41**: 1133-1144, 2014. [In Chinese]

Yang J., Kong Q., Xiang C.: Effects of low night temperature on pigments, Chl *a* fluorescence and energy allocation in two bitter gourd (*Momordica charantia* L.) genotypes. – Acta Physiol. Plant. **31**: 285-293, 2009.

Zhang D., Zhang Q.S., Yang X.Q.: Adaptive strategies of *Zostera japonica* photosynthetic electron transport in response to thermal stress. – Mar. Biol. **164**: 35, 2017.

Zhang H., Chen Y., Niu Y. *et al.*: Characterization and fine mapping of a leaf yellowing mutant in common wheat. – Plant Growth Regul. **92**: 233-247, 2020.

Zhang L.M., Lv W.Y., Zhang L.X.: [Agronomic traits and physiological-biochemical characteristics of light-green leaf mutant *sll1* of *Sorghum bicolor*.] – Plant Physiol. J. **50**: 1401-1405, 2014. [In Chinese]

Zhang Z.S., Jia Y.J., Gao H.Y. *et al.*: Characterization of PSI recovery after chilling-induced photoinhibition in cucumber (*Cucumis sativus* L.). – Planta **234**: 883-889, 2011.

Appendix. Abbreviations of the parameters of the data derived from the transient fluorescence of chlorophyll *a*.

Fluorescence parameters	Description
$M_0 = 4\,[(F_{300\mu s} - F_0)/(F_M - F_0)]$	The initial slope of the relative variable fluorescence of the relative rate at which Q_A is reduced
$W_K = (F_K - F_0)/(F_J - F_0)$	The normalized relative variable fluorescence
$V_J = (F_J - F_0)/(F_M - F_0)$	Relative variable fluorescence intensity at the J-step
$V_I = (F_I - F_0)/(F_M - F_0)$	Relative variable fluorescence intensity at the I-step
$\Psi_0 = ET_0/TR_0 = (1 - V_J)$	Probability that a trapped exciton moves an electron into the electron transport chain beyond Q_A^- (at t = 0)
$\varphi E_0 = ET_0/ABS = [1 - (F_0/F_m)]\,\Psi_0$	Quantum yield for electron transport (at t = 0)
$S_m = Area/F_v$	Normalized total complementary area above the OJIP transient
$ABS/RC = M_0\,(1/V_J)\,(1/\varphi P_0)$	Absorption flux per reaction center (RC)
$TR_0/RC = M_0\,(1/V_J)$	Trapped energy flux per RC (at t = 0)
$ET_0/RC = M_0\,(1/V_J)\,\psi E_0$	Electron transport flux per RC (at t = 0)
$DI_0/RC = (ABS/RC) - (TR_0/RC)$	Dissipated energy flux per RC (at t = 0)
$RC/CS_0 = \varphi P_0\,(V_J/M_0)\,(ABS/CS)$	Density of RCs per excited cross section (CS) (at t = 0)
$ABS/CS_0 \approx F_m$	Absorption flux per CS (at t = 0)
$TR_0/CS_0 = \varphi P_0\,(ABS/CS)$	Trapped energy flux per CS (at t = 0)
$ET_0/CS_0 = \varphi E_0\,(ABS/CS)$	Electron transport flux per CS (at t = 0)
$DI_0/CS_0 = (ABS/CS)\,(TR_0/CS)$	Dissipated energy flux per CS (at t = 0)
$PI_{ABS} = (RC/ABS)\,[\varphi P_0/(1 - \varphi P_0)]\,[\Psi_0/(1 - \Psi_0)]$	Performance index on absorption basis